44. Marine Hydrokinetic Energy Resource Assessment

Manhar R. Dhanak, Alana E.S. Duerr, James H. VanZwieten

Marine hydrokinetic energy includes that due to waves, tides, and ocean currents. The characteristics of these forms of energy and the assessment of their potential for extraction are discussed briefly herein. Detailed consideration is given to the assessment of ocean current energy, including a case study of the resource assessment of the Florida Current. Estimates of global and local open ocean current resources are obtained based on data from an ocean model. The power densities of major western boundary currents are estimated and the potential for development of ocean currents globally is assessed. Principal factors that govern economic viability of harnessing an ocean current at a location include the in-situ power density, the distance of the location from the shore, and the local depth of the seafloor. A metrics based on these considerations is discussed. Once potential sites are identified, considerations would need to be given to regulatory and permitting requirements, including assessment of potential impact on the environment and its ecosystems, marine spatial planning and the impact on the energy resource itself; development of optimal design of devices for high performance; and mitigation of deployment and maintenance costs.

44.1 **Wave Energy Resource** 1100
44.2 **Tidal and Ocean Current Energy Resource** 1101
44.2.1 Tidal Currents 1102
44.2.2 Ocean Currents 1102
44.2.3 Power and Power Density of Tidal and Ocean Currents 1104
44.3 **Assessment of Global Ocean Current Resources** 1106
44.3.1 Gulf Stream Case Study 1110
44.4 **Other Considerations** 1113
References 1114

The energy in the oceans may be classed as hydrokinetic when it is in the form of waves, and tidal and ocean currents, and as potential energy when it in the forms of thermal and salinity gradients, and tidal water levels. The prevalence of these forms of energy is geographic specific. Major ocean currents are typically western boundary currents on the eastern coasts of the continents. Tidal energy typically represents significant ocean energy resources in the estuaries and channels at a number of locations worldwide, such as the northeast of United States or the western coast of Europe. Significantly high wave energy sources are typically found in mid to high latitudes (40–60°) along coastlines facing large open oceanic regions with significant wind fetch, such as the northwest coast of the US. Thermal gradients are significant at certain locations in low to mid latitudes (0–35°). The feasibility of cost-effectively harnessing any of these forms of energy from a specific region depend on a number of factors, including the distance of the region from the shore, the local water depth, and the potential impact of harnessing the energy on the environment and on the local stakeholders. Developing just a small fraction of the available wave energy resources could allow for millions of homes to be powered.

In this chapter, we provide a brief assessment of the various forms of marine hydrokinetic energy and provide details of the methodology for estimating the potential for energy extraction in the particular case of the hydrokinetic energy of an open ocean current, together with an overview of the world's major ocean currents as significant ocean energy resources. The ocean current energy potential at identified global locations is estimated using a computational ocean model. The model's accuracy in predicting the actual current conditions and hence the resource potential is discussed. In Sect. 44.1, the potential for wave energy is discussed; in Sect. 44.2, the potential for tidal and ocean currents is discussed; in Sect. 44.3, practical considerations in extracting ocean and tidal current energy are discussed; and in Sect. 44.4, a case study for assessing extractable ocean current energy resource is discussed.

44.1 Wave Energy Resource

Waves are significant sources of hydrokinetic energy. Typically, waves generated by winds are of interest here. Waves form in a complex evolving process involving fluctuations in air pressure over a range of frequencies induced by unsteady turbulent winds, shear layer instabilities, and interaction between waves [44.1–3]. The height, period, wavelength, and direction of propagation of waves are governed by the wind velocity, wind duration, fetch – the distance over water that the wind blows along a particular direction – and water depth and bottom topography. Large waves correspond to high winds operating over long duration over considerable fetch. The absence of significant wind strength, duration, or fetch curtails the growth of waves. Waves in a given area typically have a spectrum of heights, periods, and wavelengths, from very small, short capillary waves of periods $T < 0.1\,\mathrm{s}$ to chops of wave heights of $O(0.1-10\,\mathrm{m})$ and periods $1\,\mathrm{s} < T < 10\,\mathrm{s}$ to swells of wave heights of the same order but periods in the range $10\,\mathrm{s} < T < 30\,\mathrm{s}$. While chops are associated with local winds, have relatively short wavelength and are of short duration, swells are typically generated by distant storms, are narrow banded, have longer wavelengths and travel long distances; as waves disperse from the region of the storm, shorter waves get dissipated, while longer $O(100\,\mathrm{m})$, faster traveling, waves persist over great $O(1000-10\,000\,\mathrm{km})$ distances. The wave height of a group of waves is characterized by the significant wave height, H_s. For specific wind velocity, duration, and fetch, a threshold, referred to as *fully developed seas*, is reached, whereby additional action of the wind results in breaking of wave tops and formation of *whitecaps*. Wave-induced oscillatory motion in the water column is highest at the surface and diminishes rapidly with depth.

Wave energy propagates with the group velocity. The wave energy flux per unit along crest width (wave power density), which is the mean rate of transport of the wave energy through a vertical plane of unit span along a wave crest, for unidirectional waves is given in units of W/m by

$$P_\mathrm{h} = \rho g \int_0^\infty C_\mathrm{g} S(f)\,\mathrm{d}f\,, \tag{44.1}$$

where $S(f)$ is the wave spectrum and $C_\mathrm{g}(f,d)$ is the group velocity of the harmonic wave component of frequency f Hz in waters of depth d. In the case of directional spread, we consider $S(f) = \int_{-\pi}^{\pi} S(f,\theta)\,\mathrm{d}\theta$. According to linear wave theory,

$$C_\mathrm{g} = \frac{g \tanh kd}{4\pi f}\left(1 + \frac{2kd}{\sinh 2kd}\right)\,,$$
$$(2\pi f)^2 = gk \tanh kd\,. \tag{44.2}$$

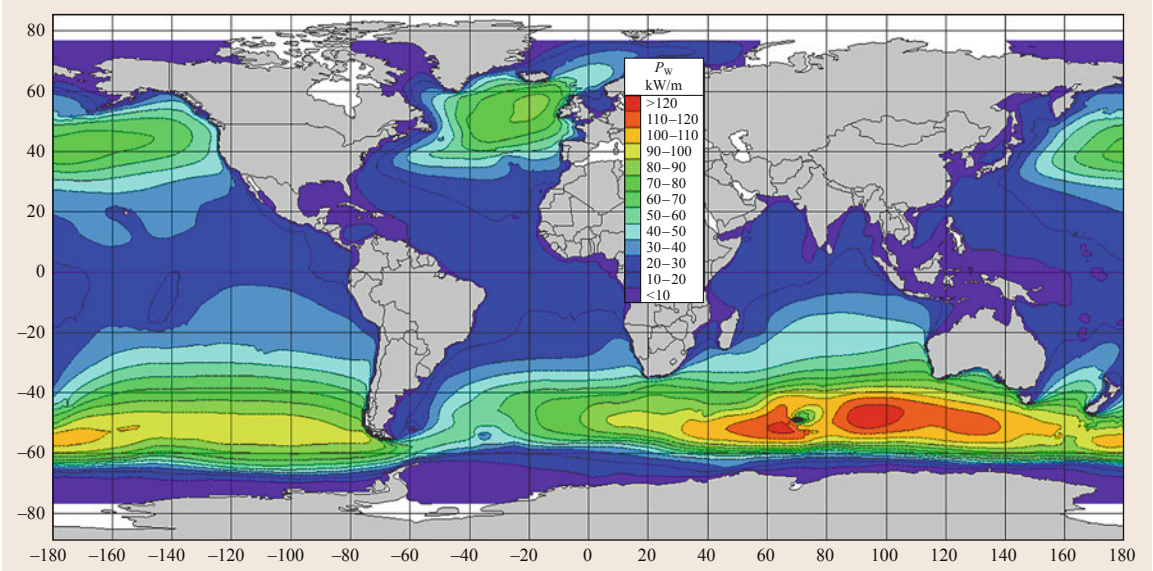

Fig. 44.1 Global distribution of annual mean wave power. Wave power density in kW/m is shown, based on NOAA WAVEWATCH-III (NWW3) wind–wave model (after [44.4])

In deep water, $C_g = \frac{g}{4\pi f}$, so that

$$P_h = \frac{\rho g^2}{4\pi} \int_0^\infty \frac{S(f)}{f}\,df = \frac{\rho g^2}{4\pi} m_{-1} = \frac{\rho g^2 H_0^2 T_e}{64\pi}\,, \tag{44.3}$$

where

$$H_0 = 4\sqrt{m_0} = 4\sqrt{\int_0^\infty S(f)\,df}$$

is the significant wave height and $T_e = \frac{m_{-1}}{m_0}$ is the wave energy period.

In shallow water, $C_g = \sqrt{gd}$ and $S(f) \to S_s(f)$, the shallow water spectrum, so that

$$P_h = \rho g \sqrt{gd} \int_0^\infty S_s(f)\,df = \frac{\rho g \sqrt{gd} H^2}{16}\,, \tag{44.4}$$

where H is the shallow-water wave height. As the waves approach the shore they undergo shoaling and refraction. Equating (44.3) and (44.4) gives the shoaling coefficient $\kappa_s = H/H_0 = (gT_e^2/(16\pi^2 d))^{\frac{1}{4}}$. In practice, some of the wave energy may be lost on approach to the shoreline through wave breaking.

As an example, consider a swell of wave energy period $T_e = 10\,s$ and wave height $H_0 = 0.5\,m$. For such a wave, (44.3) implies that the available energy is

$$P_h = \frac{\rho g^2 (2.5)}{64\pi} \simeq 1.2\,kW/m\,.$$

Figure 44.1 shows the global distribution of the annual mean available wave energy resource. As can be seen, major sources of wave energy along the continental coastlines lie on the western boundaries of the land masses in mid to high (40–60°) latitudes north and south of the Equator. In particular, northwest USA, western Europe, southern Chile, and south and west Australia have high wave power densities along their coastlines. *Gunn* and *Stock-Williams* [44.5] use NOAA Wavewatch III model [44.6] data to estimate that worldwide the total mean wave energy resource is over 2 TW or 17 532 TWh/year, with the mean resource being higher in winter than in summer in either hemisphere; they estimate that accounting for the effect of directional spread implies around 15% reduction in this estimate. Other estimates vary between 1.3 TW or 11 396 TWh/year [44.7] and 3 TW or 26 297 TWh/year [44.8]. *Gunn* and *Stock-Williams* [44.5] found that Australia (280 GW), USA (223 GW) and Chile (194 GW) have the highest potential for wave energy conversion.

The fraction of this available wave energy resource that can be extracted is based on a number of factors, including available conversion technologies, their efficiencies and packing capacities, economic viability, and environmental impact considerations. Using an example of an array of Pelamis devices, *Gunn* and *Stock-Williams* [44.5] suggest that based on current technologies, 4.6% of the 2 TW of available global wave energy may be extractable. An Electric Power Research Institute (EPRI) report [44.9] finds that technically recoverable resources for electric generation from waves around the US coastline is approximately 1170 TWh/year (134 GW), which is almost one third of the 4000 TWh of annual electricity usage in the USA.

44.2 Tidal and Ocean Current Energy Resource

Tidal currents are globally ubiquitous and together with major ocean currents represent important marine hydrokinetic sources of renewable energy. Importantly, tidal currents are highly predictable, while major ocean currents, such as the Gulf Stream and the Kuroshio Current, in a number of places around the world flow fairly persistently as part of ocean circulation systems. Therefore, tidal and ocean current energy conversion, along with solar, wind, waves, and other renewables, is an imperative consideration for a future energy portfolio for sustainability. Industry and governments worldwide are moving to invest in developing these forms of ocean energy; for example, the European Marine Energy Center (EMEC) has developed a major at-sea test facility for tidal current energy conversion devices in Orkney. A number of studies have been conducted worldwide, and various energy conversion devices have been designed and built, borrowing much of the technology from the wind industry. Since seawater is 800 times denser than air, ocean and tidal currents are energy dense, such that at low speeds they have kinetic energy per unit area comparable to that of winds of speed nearly an order of magnitude higher. For example, currents of speed 1 m/s have the same power capacity per unit area as winds of speed 9.3 m/s. Because of this physical property, ocean currents contain an enormous amount of energy that can be captured and converted to a usable form. Despite this potential, challenges remain

in research and development of efficient energy extraction devices, assessment of environmental impact, development of best practices and operating procedures, and establishment of policies and regulations.

44.2.1 Tidal Currents

Tides are very long waves, made up of harmonic constituents whose periods range from $O(1-10\times10^4\,\mathrm{hr})$, that flow to and fro between the oceans and coastlines in response to the gravitational forces exerted by the moon and the sun on the earth in combination with inertial forces, leading to the rise and fall of the sea level at the coastlines. At any coastal location, high and low tides correspond to the crest and trough of the tidal wave, respectively, reaching the location, the difference in sea levels between the two states being the tidal range at the location. The tidal range provides a good measure of the tidal energy resources at a location.

The tidal motion of the water is primarily a balance between the gravitational forces of the moon and the sun and the forces of inertia. In view of its relative proximity to the earth, the moon plays a greater role than the sun in generating the tides. The gravitational force of the moon on earth overcomes the inertial forces on the side closest to it and pulls the associated ocean into a bulge, while on the side furthest from the moon, inertial forces dominate and pull the water column away in the opposite direction, leading to a similar bulge furthest away from the moon. As the earth rotates and the moon moves around the earth and the alignment between the earth and the moon shift accordingly, the bulges maintain position with respect to the alignment causing cyclic variation in water levels over a lunar day, which is 24 hr 50 min long. If the earth were perfectly spherical and fully covered with water, this would result in semi-diurnal tides, involving two approximately equal high and two approximately equal low tides a day, everywhere. However, since the earth is not perfectly spherical and tidal flows of the oceans are interrupted by landmasses, tidal patterns are complicated. Many places, such as the east coast of the US, have semi-diurnal tides with the harmonic component M_2, of period of 12 hr, 25 min, being the major constituent of the tidal wave; other major constituents are the principal solar semi-diurnal S_2 component (12 hr period) and larger lunar elliptic semi-diurnal component (12 hr, 40 min period). Other places, such as in the Gulf of Mexico, have diurnal, or one high and one low tide a day, primarily governed by diurnal lunar components K_1 (23 hr, 56 min period), and O_1 (23 hr, 49 min period), and solar diurnal component S_1 (24 hr period). Yet other places, such as the western coast of the US, experience mixed semi-diurnal tides, involving two unequal high and two unequal low tides a day. Regionally, tidal flows are influenced by the shape of coastlines and opening to bays as well as by interactions with local riverine flows in estuaries, by weather patterns and winds as well as other currents. The tidal cycles and their amplitudes vary with time and position along a coast. During full moon and at new moon, the earth, the moon and the sun are aligned and the solar tide adds to the lunar tide, resulting in occurrence of maximum tidal ranges or *spring tides*. At first and third quarter moon, when the moon and the sun are at right angles, the lunar and solar tides act to dampen the tidal amplitudes, resulting in minimal tidal range or *neap tides*. Figure 44.2 shows the principal tidal component M_2, which is determined from satellite altimetry [44.10]. The associated tidal ranges are typically maximum at certain places near coastlines, particularly along the coast of northwest Europe, the northeast and northwest coasts of North America, the east coast of Africa, the northwest coast of Australia, southern and eastern parts of Asia, and northern and southern parts of South America. *Charlier* and *Justus* [44.11] (see also [44.12]) estimate that the theoretical mean global tidal power resource is around 3 TW, of which around 1 TW is available in shallow waters.

44.2.2 Ocean Currents

The mean flow in the ocean basins, separated by landmasses, comprises of large-scale subtropical gyres or circulation of surface currents that are set up by persistent action of prevailing winds, typically by the trade winds near the Equator and by the Westerlies at higher latitudes (see, for example, [44.14]). The subtropical gyres (Fig. 44.3), two in the Atlantic, two in the Pacific, and one in the Indian Ocean, rotate clockwise in the northern hemisphere and anticlockwise in the southern hemisphere and transport warmer waters from lower latitudes to higher latitudes and cooler waters from higher latitudes to lower latitudes. In the Atlantic, the North Equatorial Current, the Caribbean Current, the Gulf Stream (including the Loop Current in the Gulf of Mexico and the Florida Current), the North Atlantic Current, and the Canary Current mark the north Atlantic gyre, while the South Equatorial Current, the Brazil Current, the Antarctic Circumpolar Current, and the Benguela Current mark the south Atlantic gyre. In the Pacific, the North Equatorial Current, the Kuroshio Current, the North Pacific Current, and the California Current mark the north Pacific gyre, while the South Equatorial Current, the East Australian Current, the Antarctic Circumpolar Current, and the Peru Current mark the south Pacific gyre. In the Indian Ocean, the South Equatorial Current, the Agulhas Current, the

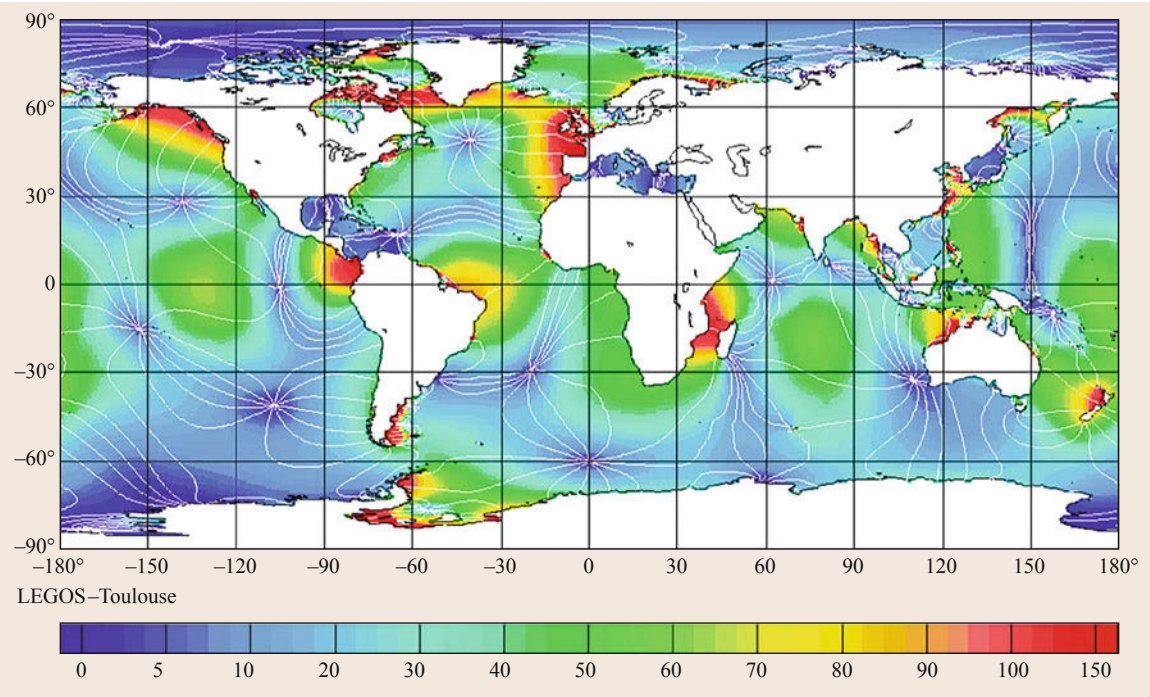

Fig. 44.2 M_2 tide (after [44.10])

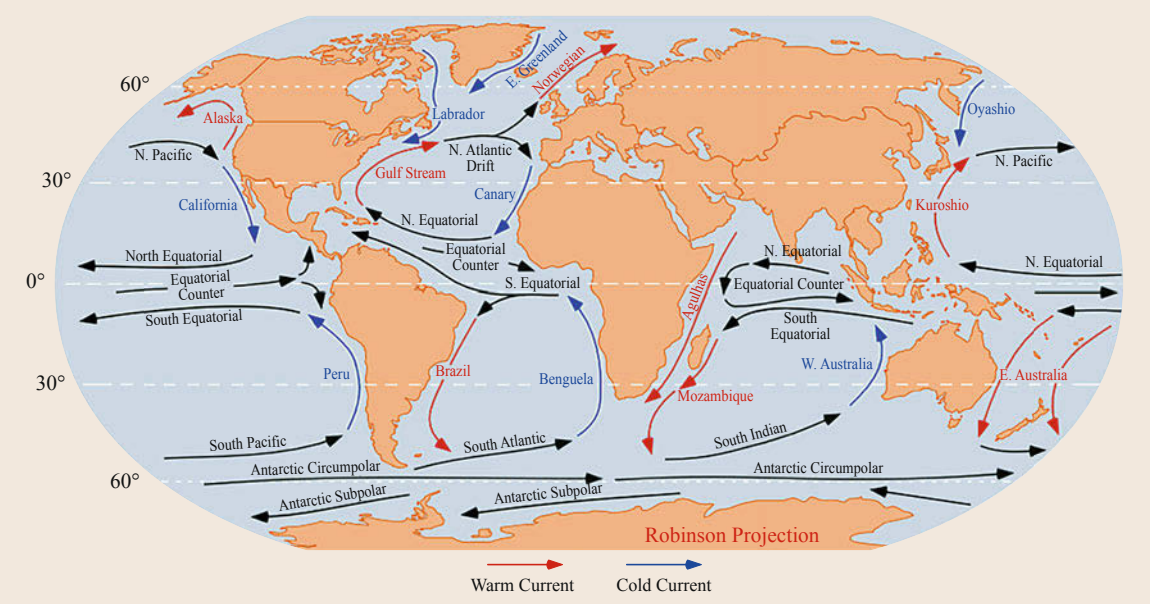

Fig. 44.3 Subtropical gyres and mean ocean currents (after [44.13])

Antarctic Circumpolar Current, and the West Australian Current mark the Indian Ocean gyre in the southern hemisphere. The landmass of the Indian subcontinent prevents full development of a gyre in the northern Indian Ocean; instead reversible currents associated with monsoon winds mark the region. In between the north and south subtropical gyres in the Atlantic and the Pacific lie Equatorial Counter Currents. Finally, smaller subpolar gyres occur, one in the North Atlantic and the other in the North Pacific.

The western arms of the subtropical gyres, referred to as *western boundary currents*, are narrow, fast, with mean speeds in the range 1–2.5 m/s, and extend deep, up to 400 m, while the eastern arms, or *eastern boundary currents*, are wide, slow, typically with mean speeds < 0.2 m/s, and shallow. The Gulf Stream and the Kuroshio Current are the most intense western boundary currents. The intensification of the western boundary currents is linked to the increasing strength of the Coriolis force as one moves away from the Equator [44.15]. The stronger Coriolis force deflects currents driven eastwards by the Westerlies south to form eastern boundary currents, which are broad so that the center of the gyre lie to the west of the basin. At lower latitudes, weak Coriolis force and the trade winds act to deflect the eastern boundary currents and transport its surface waters westwards. At the western boundary of the basin, the waters are driven towards the poles in a narrower region west of the center of the gyres, with the ocean surface sloping down westwards, thereby leading to significant contribution from the mean geostrophic flow. The time-averaged (over several days) velocity is given by the approximate equations [44.15], see also [44.16]

$$\begin{aligned}
\frac{1}{\rho}\frac{\partial p}{\partial x} &= \mathrm{g}\frac{\partial \zeta}{\partial x} = fv + \frac{\partial}{\partial z}\left(A_z \frac{\partial u}{\partial z}\right) \\
&\quad + A_H\left(\frac{\partial^2 u}{\partial x^2} + \frac{\partial^2 u}{\partial y^2}\right) , \\
\frac{1}{\rho}\frac{\partial p}{\partial y} &= \mathrm{g}\frac{\partial \zeta}{\partial y} = -fu + \frac{\partial}{\partial z}\left(A_z \frac{\partial v}{\partial z}\right) \\
&\quad + A_H\left(\frac{\partial^2 v}{\partial x^2} + \frac{\partial^2 v}{\partial y^2}\right) , \\
\frac{1}{\rho}\frac{\partial p}{\partial z} &= -\mathrm{g} ,
\end{aligned} \tag{44.5}$$

where positive x and y are along east and north directions, z points vertically upwards, and u and v are the respective horizontal components of the current velocity; p is the pressure, A_z and A_H are coefficients of eddy friction, and ζ is the mean free surface elevation.

44.2.3 Power and Power Density of Tidal and Ocean Currents

Within a column of moving fluid, the power density P_u and the available power P or hydrokinetic energy flux across a cross-sectional area A within the current may be estimated using the following equations

$$P_u(y,z,t) = \frac{1}{2}\rho U^2 (\boldsymbol{U}\cdot\boldsymbol{n}) , \tag{44.6}$$

$$P = \iint_A P_u \, \mathrm{d}A , \tag{44.7}$$

where ρ is the density of the fluid, $\boldsymbol{U}$ is the velocity of the fluid, $\boldsymbol{n}$ is the unit vector normal to the area A through which the fluid flows. If the cross-stream components of velocity can be neglected, $P_u(y,z,t) \simeq \frac{1}{2}\rho(\boldsymbol{U}\cdot\boldsymbol{n})^3$.

The power that can be extracted by a single hydrokinetic turbine may be expressed as

$$P_E = \eta P , \tag{44.8}$$

where $\eta(<1)$ is efficiency of the extraction process. In open oceans, the maximum value of η is typically estimated using the ideal, frictionless, steady incompressible flow model due to *Betz* [44.17] (see also [44.18]), where the turbine rotor is represented by an actuator disk of area A_D (Fig. 44.4). We consider the axial speed upstream, at the rotor, and downstream of the rotor to be U_1, U_D, and $U_2 = \alpha U_1 (\alpha < 1)$, respectively, each being uniform across the appropriate section within the stream tube.

Conservation of mass requires that

$$\iint_{CS} \rho\,(\boldsymbol{U}\cdot\boldsymbol{n})\, \mathrm{d}A = 0 , \tag{44.9}$$

for the fluid enclosed by the control surface CS, shown by the dashed line in Fig. 44.4; here the normal vector $\boldsymbol{n}$ points out of the volume enclosed by CS. Since $(\boldsymbol{U}\cdot\boldsymbol{n}) = 0$ along the curved sections of CS, we have

$$U_1 A_1 = U_2 A_2 = U_D A_D , \tag{44.10}$$

where A_1 and A_2 are the areas of the upstream and downstream sections of CS.

Applying the energy equation to the control volume between sections 1 and 2, we have

$$-\dot{W} = \iint_{CS} \left(\frac{1}{2}\rho U^2 + p + \rho g z\right)(\boldsymbol{U}\cdot\boldsymbol{n})\, \mathrm{d}A , \tag{44.11}$$

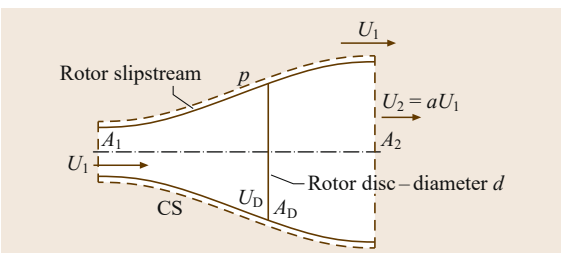

Fig. 44.4 Schematics of actuator disc model

where $\dot{W} = P_E$, is the extracted power or the work done by the fluid on the system enclosed by CS and p is the pressure. For the case of uniform flow considered here and the control surface as in Fig. 44.4, $p + \rho g z = C$, a constant over CS (using Bernoulli's equation outside of the stream tube), and (44.11) becomes

$$\begin{aligned}\dot{W} = P_E &= \left(\frac{1}{2}\rho U_1^2 + C\right) U_1 A_1 \\ &\quad - \left(\frac{1}{2}\rho U_2^2 + C\right) U_2 A_2 \,, \\ &= \frac{1}{2}\rho \left(U_1^2 - U_2^2\right) U_D A_D \,, \end{aligned} \tag{44.12}$$

using (44.10). Finally, conservation of momentum of the system enclosed by CS implies

$$\boldsymbol{F}_D = \iint_{CS} \frac{1}{2}\rho \boldsymbol{U}(\boldsymbol{U}\cdot\boldsymbol{n})\,\mathrm{d}A - \iint_{CS} (p + \rho g z)\boldsymbol{n}\,\mathrm{d}A \,, \tag{44.13}$$

where $\boldsymbol{F}_D = (-F_D, 0, 0)$ is the reaction force on the rotor to maintain it in position. Applying (44.13) to the CS in Fig. 44.4, we note that the pressure term integrates to zero so that, as in (44.10),

$$F_D = \rho(U_1 - U_2)U_D A_D \,. \tag{44.14}$$

Then extracted power P_E is also given by

$$P_E = F_D U_D = \rho(U_1 - U_2)U_D^2 A_D \,. \tag{44.15}$$

Equating (44.12) and (44.15), we obtain that the flow speed at the disk is given by

$$U_D = \frac{U_1(1+\alpha)}{2} \,, \tag{44.16}$$

where $\alpha = U_2/U_1$. Hence from (44.15), the extracted power is given by

$$P_E = \frac{1}{4}\rho U_1^3 A_D (1-\alpha)(1+\alpha)^2 \,. \tag{44.17}$$

If we regard the available reference power as $P = \frac{1}{2}\rho U_1^3 A_D$, corresponding to the energy flux through a circle of diameter A_D upstream of the disk, then the ideal efficiency of the extraction is given by

$$\eta = \frac{P_E}{\frac{1}{2}\rho U_1^3 A_D} = \frac{1}{2}(1-\alpha)(1+\alpha)^2 \,, \tag{44.18}$$

which has a maximum value of $\eta_{max} = 16/27 \approx 0.59$, when $\alpha = 1/3$ and hence $U_D = \frac{2}{3}U_1$. This maximum value is referred to as the Betz limit. Thus, maximum power that can be extracted is given by

$$P_{Emax} = \frac{1}{2}\rho U_1^3 A_D \eta_{max} \,. \tag{44.19}$$

Maximum efficiencies are lower than 0.59 when allowance is made for the finite number of blades and rotational speeds; the Betz limit is achieved only for higher values of the tip speed ratio $U_D/\Omega R_D$, where Ω is the rate of rotation and R_D is the radius of the rotor [44.19]. For nonuniform flows, the integral equations (44.9)–(44.13) must be used. Most designs for hydrokinetic turbines allow the turbine to yaw so that the turbine may be normal to the direction of the current; however, if the turbine is unable to yaw, then the full integral equations should account for the associated directional flow. Additionally, if the flow is unsteady, unsteady versions of the momentum and energy equations are needed.

Typically, tidal energy would be harnessed from tidal streams in channels and openings in coastlines or in estuaries. Therefore in making tidal energy resource assessment, consideration is given to the characteristics of the flow in such channels. *Garrett* and *Cummins* [44.20] consider an extension of (44.19) to flow in a finite tidal channel. They show that Betz limit applies when the rotor size is small compared with the channel's width. If the rotor size is comparable to the channel width, then they show that

$$P_{Emax} = \frac{\frac{1}{2}\rho U_1^3 A_D \eta_{max}}{\left(1 - \frac{A_D}{A_c}\right)^2} \,, \tag{44.20}$$

where A_c is the cross-sectional area of the channel – the efficiency of the turbine is increased due to the confining effects of the channel and associated increase in the pressure drop across the turbine. In practice, for larger blockage ratios A_D/A_c this increased efficiency needs to be balanced against the effect of increased blockage or drag on the flow that will lead to reduction in hydrokinetic energy flux [44.21]. Indeed, *Garrett* and *Cummins* [44.22] (see [44.23]), on the basis of an analysis of tidal flow in a constricted channel of variable cross-section connecting two large bodies of water, showed that if the pressure gradient in the channel is primarily balanced by frictional forces, the extractable mean power (averaged over a tidal cycle) is given by

$$P_E = 0.556\rho g a Q_m \left[1 - \left(\frac{Q_m}{Q_{0m}}\right)^2\right] \,, \tag{44.21}$$

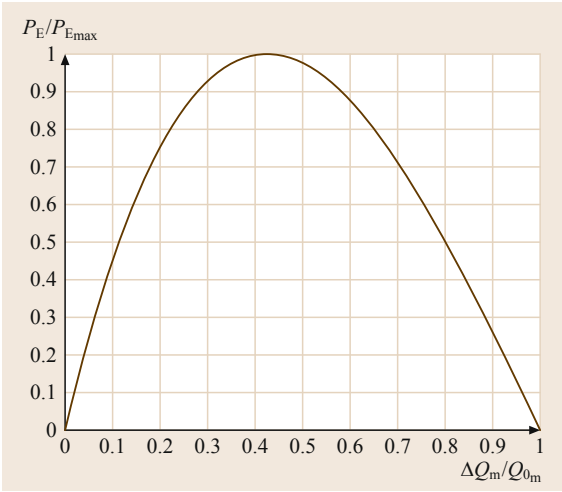

Fig. 44.5 Extracted power vs. reduction in flow rate, $\Delta Q_m = Q_{0m} - Q_m$, in the channel

where ρ is the density of water, Q_m and Q_{0m} are, respectively, the peak volume flow rates through the channel in the presence of/in the absence of power extraction, and a is the amplitude of a sinusoidal tidal head $a\cos(2\pi t/T)$ of period T between the two ends of the channel; the tidal volume flow rate is considered to be $Q = Q_m|\cos(2\pi t/T)|^{\frac{1}{2}}$. The result (44.21) is shown plotted in Fig. 44.5.

Extracting power from the tidal flow results in reduction $\Delta Q_m = Q_{0m} - Q_m$ in volume flow rate. Extractable power increases as ΔQ_m increases until

$$\Delta Q_m = \left(1 - \frac{1}{\sqrt{3}}\right) Q_{0m} = 0.42 Q_{0m}$$

(i. e., until there is 42% reduction in the flow rate), which marks the condition under which maximum mean power can be extracted from the channel,

$$P_{Emax} = 0.21\rho g a Q_{0m} \,. \tag{44.22}$$

Beyond this value of ΔQ_m, the extractable power drops to zero as $\Delta Q_m \to Q_{0m}$ or $Q_m \to 0$. If, on the basis of environmental impact considerations, a maximum of 5% reduction in channel flow rate (i. e., $\frac{\Delta Q_m}{Q_{0m}} = 0.05$) is permitted, then extraction of only 23% of the maximum extractable tidal power in the channel may be permitted. That is, $P_{EPermitted} = 0.23 P_{Emax}$.

On the basis of these considerations, and using (44.22) in a numerical simulation, *Haas* [44.24] assessed the theoretically available tidal energy resource in streams around the US coast, estimating the resource potential for tidal generation in USA to be 250 TWh/year. He showed that Alaska contains the largest number of locations with high kinetic power density, followed by Maine, Washington, Oregon, California, New Hampshire, Massachusetts, New York, New Jersey, North and South Carolina, Georgia, and Florida. The average tidal stream power density at a number of these locations exceeds $8\,kW/m^2$.

In practice, significant power extraction from tidal channels will require arrays involving thousands of turbines [44.25]. Theoretically, the power of an array of turbines can be estimated using (44.9)–(44.13); depending on the spacing of the turbines within the array, and the impact of the presence of the array and associated blockage of the overall flow of the current, the efficiency of each individual turbine will be affected [44.20, 21]. Additionally, if turbines are spaced not only cross-stream, but also upstream and downstream of each other, the wake effects of the upstream turbines will impact the inflow to the downstream turbine. This could potentially have a significant impact on the array's overall performance.

44.3 Assessment of Global Ocean Current Resources

In this section, we discuss the methodology for assessing ocean current energy resources and make an assessment of the energy potential of major ocean currents worldwide, with particular emphasis on the Florida Current [44.26–29], based on flow simulated using the Hybrid Coordinate Ocean Model (HYCOM) [44.30]. HYCOM is a data assimilative hybrid isopycnal-sigma-pressure coordinate ocean model aimed at depicting the state of the oceans at fine resolution in real time.

The 3-year time-averaged surface speeds of the global ocean currents computed using HYCOM are shown in Fig. 44.6, from which the strength of each of the major currents identified in Fig. 44.3 may be discerned. Correspondingly, regions with potential high ocean current energy resource potential can be identified from Fig. 44.6. Practical considerations, however, require that these regions be in accessible waters, generally close to shore, for cost-effective development and placement of the necessary infrastructure. On this basis, Fig. 44.6 suggests that the following regions, lying in the vicinity of the major western boundary currents, likely have good potential for development of ocean current energy: the east coast of the USA, the northeast coast of Brazil, the east and southeast coasts of Africa,

the east coasts of Japan and Taiwan, and the southeast coast of Australia.

The geostrophic components of western boundary currents may also be discerned from satellite altimetry data [44.31, 32].

As discussed in Sect. 44.2.2, major ocean currents are wind-driven surface currents that extend in a layer beneath the sea surface. The plot of time-averaged surface currents in Fig. 44.6 provides good indication of the global locations of high potential for development of ocean current energy. The actual levels of this potential also depend on the vertical extent and structure of the velocity field, which vary between the major currents and with associated geographic locations. In deep waters, the flow structure is primarily governed by baroclinic geostrophic flows associated with balance between pressure gradient forces and Coriolis force, whereas in shallower waters, frictional forces may become important, giving rise to steeper velocity gradients. The surface currents, therefore, penetrate relatively deeper in deep waters than in shallow waters; the ocean current energy resource is correspondingly higher at a site in deeper waters. The greater water depth, on the other hand, may pose challenges for installation of the infrastructure for energy extraction.

The ocean current energy flux per unit area or the power density at each node of the HYCOM computational grid may be estimated using

$$P_{\mathrm{u},i} = \overline{\frac{\rho_i}{2} U_i^3}\,, \tag{44.23}$$

where ρ_i is the seawater density and U_i the water speed at the i-th node (44.6). $P_{\mathrm{u},i}$ is averaged over the 3-year period considered. Here we compute and examine the characteristics of the power density at constant depths. In Figs. 44.7–44.11, the time-averaged power density $P_{\mathrm{u},i}$, for $P_{\mathrm{u},i} > 500\,\mathrm{W/m^2}$, is plotted globally at specified depths; $P_{\mathrm{u},i} < 500\,\mathrm{W/m^2}$ is likely to be too low to support commercial scale ocean energy extrac-

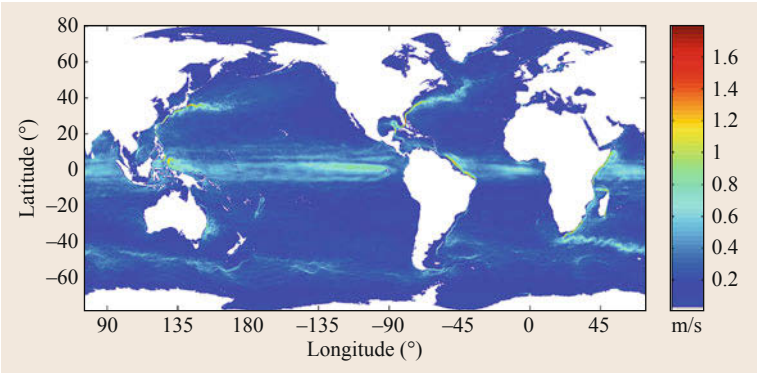

Fig. 44.6 3-year surface current average, HYCOM global model, 2009–2011

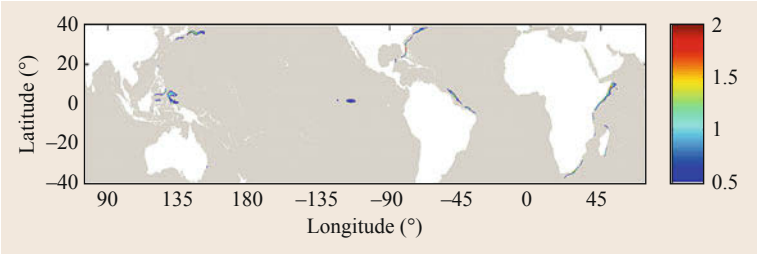

Fig. 44.7 3-year average ocean current power density at the sea surface in $\mathrm{kW/m^2}$

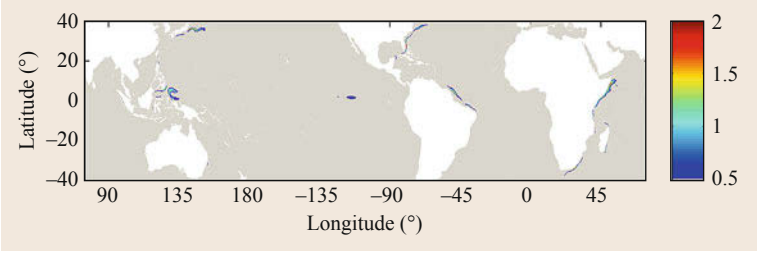

Fig. 44.8 3-year average ocean current power density at 30 m in $\mathrm{kW/m^2}$

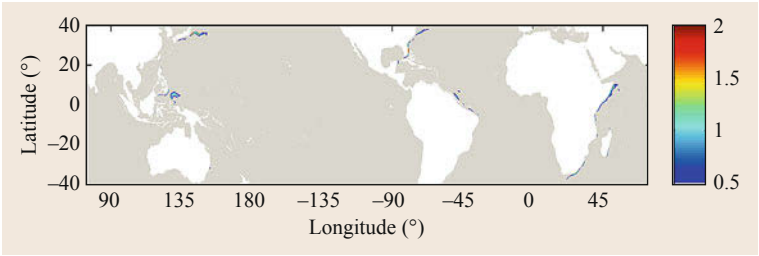

Fig. 44.9 3-year average ocean current power density at 50 m in kW/m^2

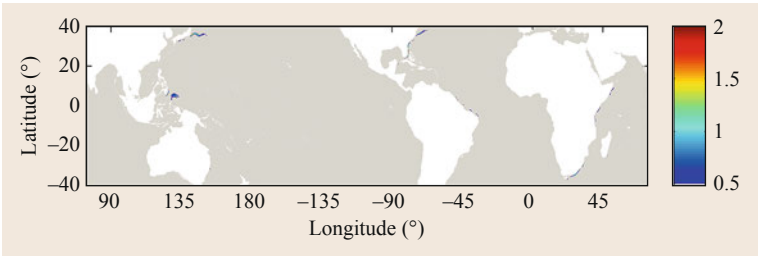

Fig. 44.10 3-year average ocean current power density at 75 m in kW/m^2

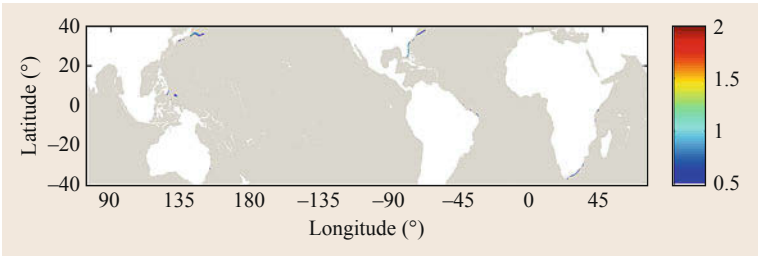

Fig. 44.11 3-year average ocean current power density at 100 m in kW/m^2

tion [44.24]. At the surface, where the current is the strongest, the power density is most dense. Since the surface currents decay with depth, the power densities decrease correspondingly, as is evident from Figs. 44.7–44.11.

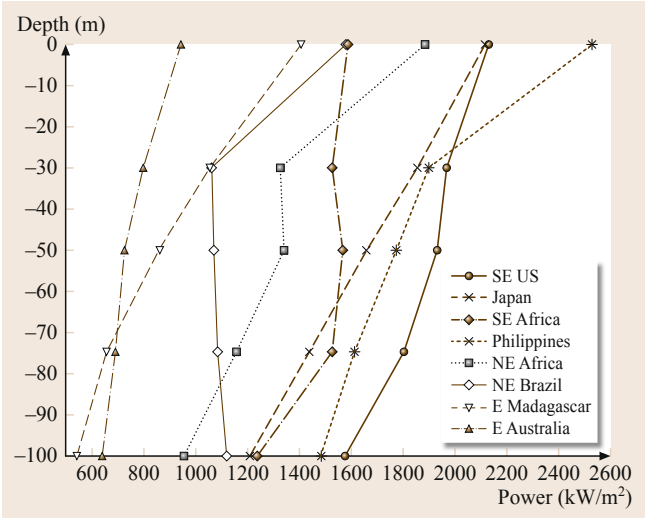

Fig. 44.12 Time average maximum power density in each region as a function of depth

Based on these plots, locations worldwide that have best ocean current energy potential are the east coast of the USA, the northeast and southeast coasts of Africa, the southeast coast of the Philippines, the eastern coast of Japan and Taiwan, the northeast coast of Brazil, the southeast coast of Africa, and the east coast of Madagascar; the corresponding currents are, respectively, the Gulf Stream (USA), the Agulhas Current (Africa), a combination of the North Equatorial, South Equatorial, and Equatorial Counter Current (the Philippines), the Kuroshio Current (Japan and Taiwan), the Southern Equatorial Current (Brazil), and the Mozambique Current (Madagascar).

The estimated maximum value of the time-averaged mean power density at various depths for each of the major ocean currents is provided in Fig. 44.12. The depth-specific maximum for each current is over the respective area where $P_{u,i} > 500\,\mathrm{W/m^2}$. The maxima are not necessarily at the same geographic points at each depth. At many of these locations, the ocean current energy potential extends to a depth of 100 m. This facilitates placement of turbine infrastructure at depths

Table 44.1 Ocean current energy extraction potential at 50 m depth

Region	Max power density [kW/m^2]	Sea floor depth [m]	Distance from shore [km]
US East Coast	1.93	500–600	57
Southeast Africa	1.66	700–800	28
The Philippines	1.57	3000–3500	32
Japan	1.78	3500–4000	116
Northeast Africa	1.34	400–500	12
Brazil	1.08	300–400	57
Madagascar	0.86	300–400	29
Australia	0.73	1400–1500	38

where impact on shipping is minimized but where the resource is still viable. It also facilitates placement of turbines with relatively large rotors.

The value of the power density is an important driving factor in choosing a viable location for turbine placement. The distance from the shore and the depth of the seafloor at the location are other factors, since they significantly determine the overall cost of designing, building, installing, and maintaining the turbine infrastructure. The length of power transmission cables and the associated costs increase the further the location is from shore. Additionally, operations and maintenance (OM) costs as well as installation costs of the turbine array at a distance from the shore increase accordingly. The depth of the ocean floor at the installation location significantly governs the type of installation required. The deeper the ocean floor, the more complicated the installation system and higher the OM costs, so that the overall costs are higher. For an installation depth of 50 m that avoids potential interference with shipping and interaction between the turbines and the free surface, the location of maximum power density, together with the associated distance from shore and the sea floor depth are compared in Table 44.1.

In Table 44.1, the highest maximum power density is 1.93 kW/m^2 and is off the US East Coast; however, it is 57 km offshore and the sea floor depth is 500–600 m. The choice of the installation location will, therefore, be a compromise between these three factors, as well as other considerations such as the state of the local electric grid infrastructure that will impact the overall economics of the installation. It is important to note that in several of these regions HYCOM predicted slightly lower power densities in much shallower water, a much more accessible resource for development; therefore a more rigorous regional site assessment, which is beyond the scope of this global analysis, is necessary. It is also important to note that HYCOM has been shown to significantly under predict the power density in some regions. For example, a measurement-based study estimates average power density of 2.2 kW/m^2 at 20 m-depth level at a location off South Africa, where the sea floor depth is approximately 100 m [44.33]. A second measurement-based study estimates average power density of 3.0 kW/m^2 at a 50 m-depth level off Florida [44.34]. These studies highlight the importance of conducting corroborative measurement based analyses.

Another factor of interest is the areal extent at an identified region over which viable hydrokinetic energy potential exists. In Table 44.2, average statistics for the area over which a given power density threshold is met are presented for the global currents 50 m-depth level. Additionally, the average power density over the region in which energy extraction may be viable – namely where the average power density is greater than 500 W/m^2 – is estimated.

An economics metric can be created to compare the energy development potential at these sites. A average power density and maximum power density would be positive factors in the economics metric of current energy development, while depth and distance from shore

Table 44.2 Area available for ocean current energy development at various locations at an operating depth-level of 50 m (1000 km^2)

Region	Area with power density greater than threshold (in ×1000 km^2)					
	> 500 W/m^2	> 750 W/m^2	> 1000 W/m^2	> 1500 W/m^2	> 2000 W/m^2	Average power density in area with $P_{u,i}$ > 500 W/m^2 [W/m^2]
Gulf Stream	147	51	25	7	0	776
SE Africa	71	28	14	0	0	765
The Philippines	194	89	9	1	0	744
Japan	172	72	37	6	0	792
NE Africa	183	37	2	0	0	661
Brazil	57	3	0	0	0	599
Madagascar	9	1	0	0	0	645
Australia	4	0	0	0	0	582

Table 44.3 Example global ocean current energy potential economics metric F, with all weighting factors = 1

Location	F
Gulf Stream	7058
SE Africa	4276
The Philippines	2190
Japan	558
NE Africa	28911
Brazil	1861
Madagascar	466
Australia	33

would be negative factors. As the positive factors increase, so does the economic outlook of the array, and as the negative factors increase, the economic outlook of energy development at the site decreases. An example metric may be

$$F = \frac{(A\alpha)(P_{\text{umax}}\beta)(P_{\text{umean}}\gamma)}{(D\zeta)(d\xi)} , \qquad (44.24)$$

where A is the area over which the average power density is greater than 500 W/m^2 in units of 1000 km^2, α is the weighting factor for A in km^{-2}, $P_{\text{umax}} = \overset{\max}{i}\{P_{\text{u},i}\}$ is the maximum power density in W/m^2, β is the weighting factor for P_{umax} in m^2/W, $P_{\text{umean}} = \frac{1}{N}\sum_{i=1}^{N} P_{\text{u},i}$ is the mean power density within area A in W/m^2, γ is the weighting factor for P_{umean} in m^2/W, D is the distance from shore in km, ζ is the weighting factor for D in km^{-1}, d is the depth of the sea floor in m, and ξ is the weighting factor for d in m^{-1}. Using this example metric, and assuming that the weighting factors all have a numerical value of 1, the results for the global currents at 50 m are given in Table 44.3.

With all the weighting factors set to 1, the metric suggests that Northeast Africa is the best global location for hydrokinetic energy development, the metric being heavily biased by the distance of the potential from the shore (12 km). This metric can be modified not only by selecting other weighting factors, which were set to 1 in the case considered above, but also by changing the factors considered in the metric. Additional factors can be added or removed from this metric depending on the initial economic evaluation of the turbine array.

44.3.1 Gulf Stream Case Study

As an example, the Gulf Stream off the east coast of the United States is considered further for its hydrokinetic resources using the HYCOM Gulf of Mexico basin model data [44.26, 27]. The time-averaged power densities for various depths are plotted in Figs. 44.13–44.17. The figures highlight the power density decay with

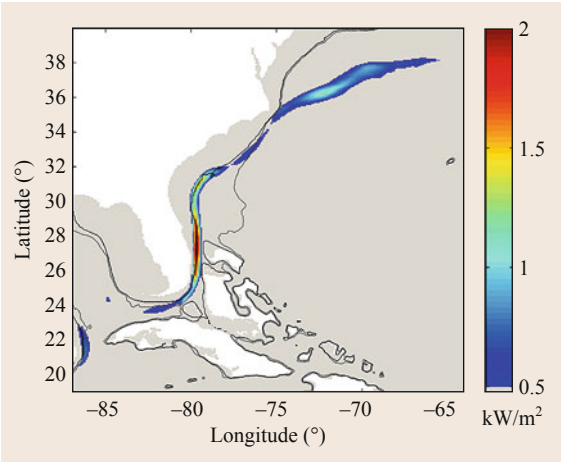

Fig. 44.13 3-year average power density of the Florida Current at the surface

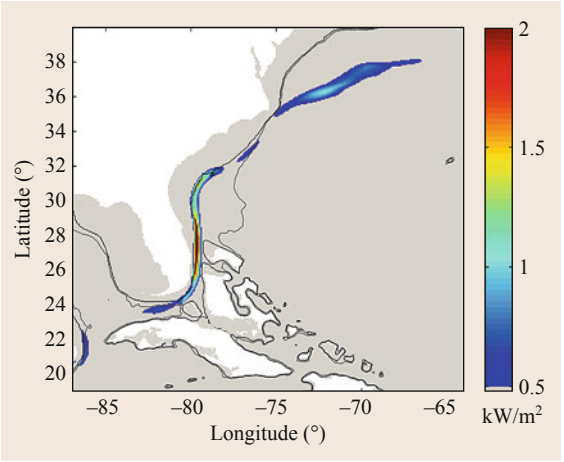

Fig. 44.14 3-year average power density of the Florida Current at 30 m

depth. This is especially apparent in comparing the plot for the power density at the surface (Fig. 44.13) with that at 100 m (Fig. 44.17). As seen in the figures, the highest power density in the Gulf Stream is off the east coast of Florida, corresponding to the Florida Current – the portion of the Gulf Stream that flows off the east coast of Florida. The proximity to large population centers, including Miami, Fort Lauderdale, and West Palm Beach, make the Florida Current an attractive energy resource for the state of Florida. Figure 44.18 highlights the relationship between latitude and power density in this region, suggesting that the latitude with the highest power density is approximately 27°N.

The factors that govern resource assessment are shown in Table 44.4. It may be noted that the location of the maximum power density at the surface is

Table 44.4 Gulf Stream hydrokinetic resource assessment factors (based on HYCOM data [44.26, 27])

Depth [m]	Location		Power density [kW/m^2]	Average power density in area with $P_{u,i} > 500$ W/m^2 [W/m^2]	Sea floor depth [m]	Distance from shore [km]
	Latitude, °N	Longitude, °E				
0	27.09	−79.76	2.13	797	400–500	35
30	27.45	−79.68	1.97	782	500–600	57
50	27.45	−79.68	1.93	776	500–600	57
75	27.45	−79.68	1.81	762	500–600	57
100	27.45	−79.68	1.58	739	500–600	57

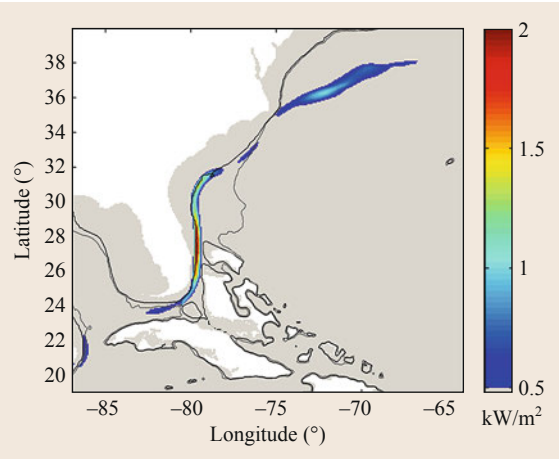

Fig. 44.15 3-year average power density of the Florida Current at 50 m

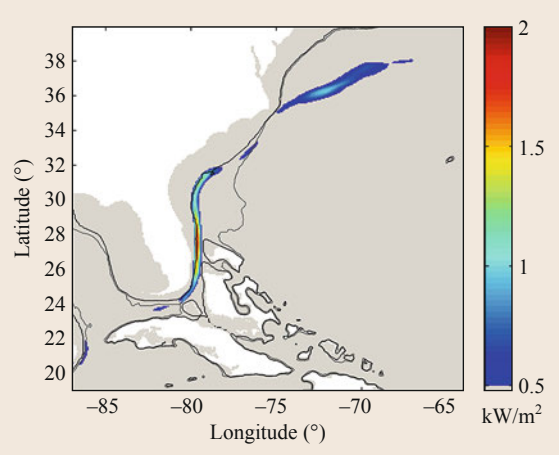

Fig. 44.16 3-year average power density of the Florida Current at 75 m

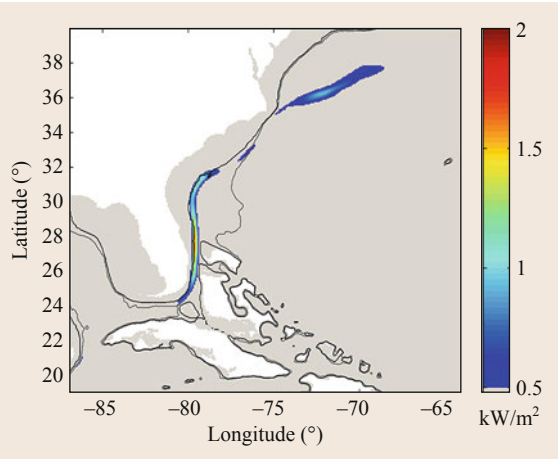

Fig. 44.17 3-year average power density of the Florida Current at 100 m

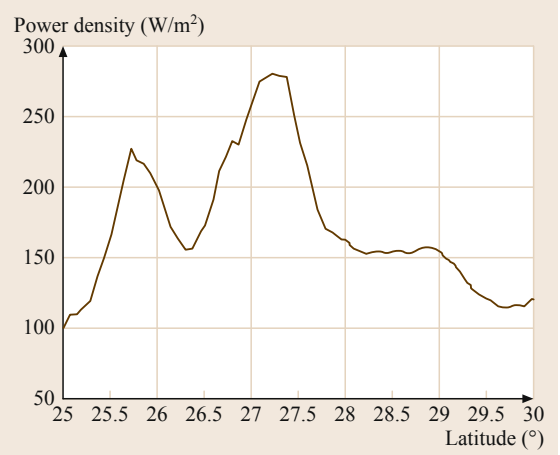

Fig. 44.18 Variation in Florida Current power density with latitude

different from the location of the corresponding values at depths between 20 and 100 m. This suggests that use of power density based on surface current data in site selection may be misleading, since turbine arrays would be installed at some depth below the water surface. The maximum power densities at 30, 50, 75, and 100 m depth are at a location 40 km away. The maximum power densities at these depths are at the same geographic location within the Florida Current; however, this may not happen in every global current. Care

is needed in making the resource assessment and deciding on optimal locations. The type and size of devices used and the water depth at which they operate optimally will dictate the depth at which a detailed resource assessment would be required.

Based on this overall assessment, the best location in the Florida Current for hydrokinetic energy extraction seems to be at 27.45°N, 79.76°W. However, use of the metric (44.21) may suggest an alternative location as being more desirable. A method for finding an ideal location in the Florida Current is suggested by *Duerr* [44.26], based on consideration of the variability of the hydrokinetic resource with latitude rather than water depth. The Florida Current is divided into constant latitude cross-sections to evaluate the hydrokinetic power over the entire cross-section, as in (44.7). In addition to the hydrokinetic power, the hydrokinetic power density, the depth at the core of the current, and the distance of the core from the shore are evaluated at each cross-section from 25 to 30°N.

The economics metric in this case is slightly modified from (44.24)

$$F = \frac{(A\alpha)(P\beta)(P_{\text{umean}}\gamma)}{(D\zeta)(d\xi)} , \tag{44.25}$$

where the P_{umax} term in (44.24) has been replaced with P, the average power at the cross-section in GW, and the unit of β is adjusted accordingly to GW^{-1}. The values of the metric F based on the HYCOM data, with the weighting factors set to 1 as before and with D now given by the location of the core of the current, are shown in Table 44.5.

This economics metric suggests that 26.95°N is the best latitude for hydrokinetic energy extraction. This

Table 44.5 Florida hydrokinetic resource assessment factors based on constant latitude cross-section analysis (using HYCOM data)

Latitude [°N]	Power [GW]	Mean power density [W/m^2]	Depth [m]	Distance [km]	Area with power density > 500 W/m^2 [km^2]	Metric F
25.51	8.1	164.8	700	30	5.28	0.33
25.66	9.0	209.1	700	32	6.15	0.51
25.80	9.5	218.4	700	33	6.61	0.59
25.95	9.6	207.9	600	34	6.73	0.66
26.09	9.6	183.3	500	35	6.70	0.68
26.23	9.7	163.0	500	36	6.71	0.59
26.38	10.2	156.3	500	29	6.89	0.76
26.52	10.3	173.5	400	29	6.91	1.08
26.66	10.6	211.5	400	29	7.03	1.36
26.81	11.0	233.1	400	29	7.27	1.60
26.95	11.5	248.3	400	29	7.58	1.89
27.09	11.9	275.7	400	37	7.84	1.75
27.23	12.2	280.4	500	46	8.06	1.21
27.37	12.3	278.6	500	54	8.19	1.05
27.52	12.4	232.5	500	54	8.18	0.88
27.66	12.2	199.6	500	62	8.10	0.64
27.80	12.3	169.8	600	70	7.97	0.40
27.94	12.4	163.6	500	77	7.94	0.41
28.08	12.4	157.4	500	77	7.88	0.40
28.22	12.4	153.1	400	84	7.87	0.44
28.36	12.6	154.1	400	83	7.91	0.46
28.51	12.7	153.9	400	75	7.92	0.52
28.65	12.8	153.3	400	82	8.07	0.49
28.79	13.0	155.7	500	96	8.15	0.35
28.93	13.1	156.4	500	102	8.20	0.33
29.07	12.9	149.5	600	109	8.09	0.24
29.21	12.7	141.2	600	115	7.98	0.21
29.35	12.4	127.5	600	121	7.80	0.17
29.49	12.2	121.0	700	127	7.63	0.13
29.62	12.1	115.7	700	126	7.46	0.12
29.76	11.9	115.1	700	132	7.28	0.11
29.90	11.7	115.4	700	132	7.12	0.10
30.04	11.7	123.6	600	140	7.02	0.12

is only one method of calculating a suitable metric, and other factors can be introduced into the equation. Overall, based on the constant-latitude economics metric (44.25) and the constant-depth economics metric (44.21), Florida Current's viable resource seems to be located between 26.45 and 27.45°N. These results, based on the ocean model, would need to be complemented by comprehensive in-situ surveys and in-depth studies to determine any discrepancies between the ocean models and in-situ data.

Overall, present-day ocean models based on data assimilation, such as HYCOM, provide excellent predictions of oceanic flows. However, care is needed when using ocean models. For instance, coarseness of the model grid may result in under or over prediction of, say, the speed of a current or the associated volume flow rate and correspondingly under or over-prediction of its hydrokinetic energy resource. Comparing the data from an ocean model with in-situ measurements is, therefore, essential in validating the predictions of the model. Once such deficiencies in the ocean model have been identified and characterized, the resource prediction can be better qualified. Local models with refined grids may be considered for improvement of the model.

While HYCOM is one of the most widely used ocean models, the velocity predictions of the global model are not perfect for ocean energy resource assessment. In both the Florida Current [44.28] and off the coast of Brazil [44.35], it has been shown that the HYCOM global model under-predicts the current velocities. While the overall trend in the difference between the in-situ data and the HYCOM is the same in both studies, the *Jeans* et al. [44.35] study suggests that HYCOM's prediction off Brazil is highly uncorrelated with the in-situ data, while the *Duerr* et al. [44.28] study suggests that HYCOM predicts the overall trend in the velocity data well – that is, the shape of the velocity profile predicted by HYCOM is very similar to the in-situ observations – but under-predicts the value of maximum velocity.

The applicability of an ocean model of sufficiently fine resolution to different global locations and oceanic conditions needs to be studied in order that hydrokinetic energy predictions based on the model can be suitably qualified. In *Duerr* et al. [44.28], it is suggested that a gain term – calculated using in-situ and model data – may be applied to the HYCOM data in order to improve the agreement between the model and physical conditions. This process is straightforward if in-situ field observations of currents are available. However, in the absence of such data, the details of the ocean model should be considered in order to understand possible implications in using the model for hydrokinetic resource assessment.

44.4 Other Considerations

A number of other considerations are involved in assessment of marine hydrokinetic energy resources. These include:

- *Design of devices and technologies*. To optimize performance while minimizing environmental impact at a specific site, special consideration is needed in designing devices and arrays of devices in light of prevailing local conditions. These factors could also be introduced in the metrics (44.21), (44.25). Particular considerations include:
  - Material selection, corrosion and bio-fouling control, and advanced coatings for devices and their components
  - Assessment of hydrodynamic loads and cavitation
  - Effect of shear and turbulence on hydrodynamic performance
  - Device machinery, generators and power takeoff systems
  - Optimization in design of single and arrays of devices through modeling and simulation
  - Flow and wake interactions in arrays of devices.
- *Deployment and operations*. Robust device deployment systems and low OM costs are required for viable ocean energy development. Special considerations are needed for:
  - The choice of mooring systems and offshore platforms
  - Access requirements for the devices for planned and unplanned maintenance
  - Implementation of smart machine condition monitoring for system reliability
  - Modeling and simulation studies to assess maintenance costs.
- *Environmental impact*. Regulatory agencies require that before permission to begin marine hydrokinetic ocean energy development can be granted, an assessment of the environmental impact the activity may cause needs to be made. It is expected that the activity will not have zero impact, but will require consideration of ways of mitigating the impact. Typical issues that arise are:
  - Impact on aquatic life and mortality around devices
  - Operational and construction noise

- Electromagnetic field emissions from device infrastructure and transmission cables
- Impact on shipping, protected sites and naval operations
- Impact on road traffic and other shore activities in the vicinity ocean energy development
- Impact on energy resource. In the case of ocean currents, determination of the potential effects of energy extraction on the ocean circulation systems.

- *Socio-economics of marine hydrokinetic energy*. Economic and social issues associated with the energy development, marine spatial planning and the social acceptability of the energy extraction technologies and their implementation, including their sustainability, are significant considerations in determining viability of the resource. These include:
  - Cost of electricity compared with other sources
  - Concerns with impact of the energy technologies on stakeholder activities and their livelihood
  - Political and social will.

Based on these considerations, an iterative process may result in making the final selection of a suitable location that has the desired attributes.

References

44.1 O.M. Phillips: On the generation of waves by turbulent wind, J. Fluid Mech. **2**(5), 417–445 (1957)

44.2 J.W. Miles: On the generation of surface waves by shear flows, J. Fluid Mech. **3**(2), 185–204 (1957)

44.3 K. Hasselmann, T.P. Barnett, E. Bouws, H. Carlson, D.E. Cartwright, K. Enke, J.A. Ewing, H. Gienapp, D.E. Hasselmann, P. Kruseman, A. Meerburg, P. Müller, D.J. Olbers, K. Richter, W. Sell, H. Walden: Measurements of wind-wave growth and swell decay during the Joint North Sea Wave Project (JONSWAP), Dtsch. Hydrogr. Z **1**(8), 1–95 (1973)

44.4 A. Cornett: A global wave energy resource assessment, Proc. 18th ISOPE Conf. (2008)

44.5 K. Gunn, C. Stock-Williams: Quantifying the global wave power resource, Renew. Energy **44**, 296–304 (2012)

44.6 H.L. Tolman: User manual and system documentation of WAVEWATCH-III, Version 2.22, NOAA/NWS/NCEP/MMAB Technical Note (2002)

44.7 R. Boud, T.W. Thorpe: Wavenet: Results from the work of the European thematic network on wave energy, ERK5-CT-1999-20001, European Community (2003) pp. 307–308

44.8 G. Mørk, S. Barstow, A. Kabuth, T. Pontes: Assessing the global wave energy potential, Proc. 29th Int. Conf. Ocean Offshore Mech. Arct. Eng. (ASME) (2010)

44.9 G. Hagerman, G. Scott: *Mapping and Assessment of the United States Ocean Wave Energy Resource, Tech. Rep. 1024637* (Electric Power Research Institute, Palo Alto 2011)

44.10 AVISO: Sun and Moon shape tides on Earth, Published online October, 2000. http://www.aviso.oceanobs.com/en/news/idm/2000/oct-2000-sun-and-moon-shape-tides-on-earth/index.html

44.11 R.H. Charlier, J.R. Justus: *Ocean Energies: Environmental, Economic and Technological Aspects of Alternative Power Sources*, Elsevier Oceanography Series (Elsevier, Amsterdam 1993)

44.12 A. Lewis, S. Estefen, J. Huckerby, W. Musial, T. Pontes, J. Torres-Martinez: Ocean energy. In: *IPCC Special Report on Renewable Energy Sources and Climate Change Mitigation*, ed. by O. Edenhofer, R. Pichs-Madruga, Y. Sokona, K. Seyboth, P. Matschoss, S. Kadner, T. Zwickel, P. Eickemeier, G. Hansen, S. Schlömer, C. von Stechow (Cambridge Univ. Press, Cambridge 2011)

44.13 M. Pidwirny: Surface and subsurface ocean currents: Ocean current map. In: *Fundamentals of Physical Geography*, 2nd edn. (eBook) http://www.physicalgeography.net/fundamentals/8q_1.html (2006)

44.14 A.E. Gill: *Atmosphere-Ocean Dynamics*, International Geophysics Series, Vol. 30 (Oxford Academic Press, Oxford 1982)

44.15 W.H. Munk: On the wind-driven ocean circulation, J. Meteorol. **7**(2), 79–93 (1950)

44.16 R.H. Stewart: *Introduction to Physical Oceanography*, http://oceanworld.tamu.edu/resources/ocng_textbook/PDF_files/book_pdf_files.html

44.17 A. Betz: Das Maximum der theoretisch möglichen Ausnützung des Windes durch Windmotoren, Z. Gesamte Turbinenwesen **26**, 307–309 (1920)

44.18 G.A.M. Van Kuik: The Lanchester–Betz–Joukowsky limit, Wind Energy **10**, 289–291 (2007)

44.19 V.L. Okulov, J.N. Sørensen: Refined Betz limit for rotors with a finite number of blades, Wind Energy **11**, 415–426 (2008)

44.20 C. Garrett, P. Cummins: The efficiency of a turbine in a tidal channel, J. Fluid Mech. **588**, 243–251 (2007)

44.21 T. Nishino, R.H.J. Willden: The efficiency of an array of tidal turbines partially blocking a wide channel, J. Fluid Mech. **708**, 596–606 (2012)

44.22 C. Garrett, P. Cummins: The power potential of tidal currents in channels, Proc. R. Soc. A. **461**, 2563–2572 (2005)

44.23 G. Sutherland, M. Foreman, C. Garrett: Tidal current energy assessment for Johnstone Strait, Vancouver Island, Proc. Inst. Mech. Eng, J. Power Energy A. **221**(2), 147–157 (2007)

44.24 K.A. Haas, H.M. Fritz, S.P. French, B.T. Smith, V. Neary: *Assessment of Energy Production Poten-*

tial from Tidal Streams in the United States: Final Report (Georgia Tech Research Corporation, Savannah 2011)

44.25 T.A.A. Adcock, S. Draper, G.T. Houlsby, A.G.L. Borthwick, S. Serhadlıoğlu: The available power from tidal stream turbines in the Pentland Firth, Proc. R. Soc. A **469**(2157), 20130072 (2013)

44.26 A.E.S. Duerr: A Hydrokinetic Resource Assessment Of the Florida Current, Ph.D. Thesis (Florida Atlantic University, Boca Raton 2012)

44.27 A.E.S. Duerr, M.R. Dhanak: An assessment of the hydrokinetic energy resource of the Florida Current, IEEE J. Ocean. Eng. **37**, 281–293 (2012)

44.28 A.E. Duerr, M.R. Dhanak, J.H. Van Zwieten: Utilizing the hybrid coordinate ocean model for the assessment of Florida Current's hydrokinetic renewable energy resource, Mar. Technol. Soc. J. **46**(5), 24–33 (2012)

44.29 J.H. Van Zwieten Jr., A.E.S. Duerr, G.M. Alsenas, H.P. Hanson: Global ocean current energy assessment: An initial look, Proc. 1st Mar. Energy Technol. Symp. (METS) (2013)

44.30 E.P. Chassignet, H.E. Hurlburt, E.J. Metzger, O.M. Smedstad, J. Cummings, G.R. Halliwell, R. Bleck, R. Baraille, A.J. Wallcraft, C. Lozano, H.L. Tolman, A. Srinivasan, S. Hankin, P. Cornillon, R. Weisberg, A. Barth, R. He, F. Werner, J. Wilkin: US GODAE: Global ocean prediction with the hybrid coordinate ocean model (HYCOM), Oceanography **22**(2), 64–75 (2009)

44.31 N. Maximenko, P. Niiler, M.-H. Rio, O. Melnichenko, L. Centurioni, D. Chambers, V. Zlotnicki, B. Galperin: Mean dynamic topography of the ocean derived from satellite and drifting buoy data using three different techniques, J. Atmos. Oceanic Technol. **26**(9), 1910–1919 (2009)

44.32 P. Knudsen, R. Bingham, O. Andersen, M.-H. Rio: A global mean dynamic topography and ocean circulation estimation using a preliminary GOCE gravity model, J. Geod. **85**, 861–879 (2011)

44.33 J.H. VanZwieten Jr., I. Meyer, G.M. Alsenas: Evaluation of HYCOM as a tool for ocean current energy assessment, Proc. 2nd Mar. Energy Technol. Symp. (METS) (2014)

44.34 J.H. VanZwieten Jr., W.E. Baxley, G.M. Alsenas, I. Meyer, M. Muglia, C. Lowcher, J. Bane, M. Gabr, R. He, T. Hudon, R. Stevens, A.E.S. Duerr: Ocean current turbine mooring considerations, Proc. Offshore Technol. Conf. (2015), OTC-25965-MS

44.35 G. Jeans, L. Harrington-Missin, C. Herry, M. Prevosto, C. Maisondieu, J.A.M. Lima: Deepwater current profile data sources for riser engineering offshore Brazil, Proc. 31st Conf. Ocean Offshore Arct. Eng. (ASME) (2012), OMAE2012-83400